Tomographic three-dimensional imaging of a biological specimen using wavelength-scanning digital interference holography

M. K. Kim
Dept. of Physics, University of South Florida, Tampa, FL 33620
myungkim@chuma.cas.usf.edu

Abstract: The principle of wavelength-scanning digital interference holography is applied to three-dimensional imaging of a small biological specimen. The images are reconstructed from a number of holograms digitally recorded while the wavelengths are varied at regular intervals, and the numerical interference of the multiple three-dimensional hologram fields results in tomographic images with narrow axial resolution.An animated three-dimensional model of the object is constructed from the tomographic images.

OCIS codes: (110.6960) Tomography; (090.1760) Computer holography; (110.6880) Three-dimensional image acquisition

References and Links
1. R.A. Robb, *Three-Dimensional Biomedical Imaging*, (Wiley, John & Sons, New York, 1997).
2. C.J.R. Sheppard and D.M. Shotton, *Confocal Laser Scanning Microscopy*, (Springer, New York, 1997).
3. D. Huang, E.A. Swanson, C.P. Lin, et al., "Optical coherence tomography," Science **254**, 1178-81 (1991); A.M. Rollins, R. Ung-Arunyawee, A. Chak, et al., "Real-time *in vivo* imaging of human gastrointestinal ultrastructure using endoscopic optical coherence tomography with a novel efficient interferometer design," Opt. Lett. **24**, 1358-60 (1999).
4. P. Hariharan, *Optical Holography*, (Cambridge U. Press, Cambridge, 1996).
5. L. Yaroslavsky and M. Eden, *Fundamentals of Digital Optics*, (Birkhäuser, Boston, 1996).
6. E. Cuche, F. Bevilacqua, and C. Depeursinge, "Digital holography for quantitative phase-contrast imaging," Opt. Lett. **24**, 291-3 (1999); S. Seebacher, W. Osten, and W. Jüptner, "Measuring shape and deformation of small objects using digital holography," Proc. SPIE, **3479**, 104-15 (1998).
7. S. Trester, "Computer simulated holography and computer generated holograms," Am. J. Phys. **64**, 472-8 (1996); R. Piestun, J. Shamir, B. Wesskamp, and O. Brynagdahl, "On-axis computer-generated holograms for three-dimensional display," Opt. Lett. **22**, 922-4 (1997).
8. T.C. Poon, K.B. Doh, B.W. Schilling, "Three-dimensional microscopy by optical scanning holography," Opt. Eng. **34**, 1338-44 (1995);T. Zhang and I. Yamaguchi, "Three-dimensional microscopy with phase-shifting digital holography," Opt. Lett. **23**, 1221-3 (1998).
9. M.K. Kim, "Wavelength-scanning digital interference holography for optical section imaging," Opt. Lett. **24**, 1693-5 (1999).
10. E. Arons, D. Dilworth, M. Shih, and P.C. Sun, "Use of Fourier synthesis holography to image through inhomogeneities," Opt. Lett. **18**, 1852-4 (1993).
11. F. Le Clerc and L. Collot, "Numerical heterodyne holography with two-dimensional photodetector arrays," Opt. Lett. **25**, 716-8 (2000).

1. Introduction

Tomographic imaging obviously has important applications in biomedical and materials sciences, and numerous methods have been developed that employ wide range of spectra of electromagnetic waves or other sources. A basic strategy in many of these techniques is the detection of angular position or propagation distance (time of flight) of return signal using detector arrays or a single scanning detector. The set of angular and distance data for varying source positions is then used to calculate the three-dimensional coordinates of the object

#23554 - $15.00 US Received September 12, 2000; Revised October 17, 2000

points. This is the case with x-ray computed tomography, magnetic resonance imaging, positron emission tomography, and ultrasound imaging, as well as some of the optical tomographic methods[1]. The optical tomography is most useful in microscopic imaging because of the short wavelength and the limited penetration depth of most biological surfaces. For example, the laser confocal microscopy[2] utilizes aperturing of both the illuminated sample volume and of the detector, thereby rejecting all scattered light other than from the focal volume. More recent development of the optical coherence tomography[3] is basically a time-of-flight measurement technique, utilizing ultrashort laser pulses or continuous wave laser of very short coherence time. In both of these methods the signal is detected one pixel at a time and the three-dimensional image is reconstructed by scanning the three dimensions pixel by pixel. Although microscanning using piezzo actuators is a remarkable art, being able to obtain images frame by frame will have obvious technical advantages.

By recording the phase as well as intensity of light wave, holography allows reconstruction of the images of three-dimensional (3D) objects, and gives rise to a host of metrological and optical processing techniques[4]. With the advance of computer and electronic imaging technology, it is now very practical and often advantageous to replace portions of the holographic procedures with electronic processes[5]. For example, in digital holography the hologram is imaged on a CCD array, replacing the conventional photographic plates. The digitally converted hologram is stored in a computer and its diffraction is numerically calculated to generate simulation of optical images. With digital holography, real-time processing of the image is possible and the phase information of the reconstructed field is readily available in numerical form, greatly simplifying metrological applications[6]. Digital holograms for display applications have been limited by available CCD format size and computer memory and speed requirements, but these factors are rapidly improving[7]. On the other hand, for the purpose of tomographic imaging, although the hologram produces 3D image of the optical field, this does not by itself yield the tomographic distance information from the object surface points, other than by focussing and defocusing of the object points, which is really a subjective decision[8]. The distance information can be obtained in time-of-flight type of measurements, as stated above, or it can also be determined by counting the number of wavelengths or some multiples of it, which is the basis of various interference techniques. A well-known technique is the interference of two holograms recorded at two different wavelengths, resulting in a contour interferogram with the axial distance between the contour planes inversely proportional to the difference in wavelengths. In digital holography, it is possible to extend the process to recording and reconstruction of many holograms without introducing any wavelength mismatch or crosstalk. If a number of regularly spaced wavelengths are used for recording and reconstruction, then the peaks of the cosine squared intensity variation of the two-wavelength interference become sharper and narrower, as when a number of cosines with regularly spaced frequencies are added.

The author has recently proposed a novel digital holographic method that allows distance, or axial, resolution of objects by superposition of a number of numerically reconstructed optical diffraction fields of digital holograms that are optically recorded with varying wavelengths[9]. The principle of wavelength-scanning digital interference holography is now applied to imaging of 3D objects with diffuse surfaces, such as a biological specimen. The head part of a small insect of a few millimeters in size is imaged with 120 μm axial resolution and ~20 μm lateral resolution. An animated 3D numerical model is generated of the object's surface structure, from the tomographic data with good fidelity.

2. Principles of wavelength-scanning digital interference holography

To outline the principle of wavelength-scanning digital interference holography, we start by stating that one of the diffracted fields of a hologram, E_i, recreates an exact replica of the object wave, E_o. So we consider an object point P located at (x_o, y_o, z_o) that emits a Huygens spherical wavelet proportional to $A(\mathrm{P})\exp(ikr_P)$ measured at an arbitrary point Q located at (x, y, z), where $r_P = n\,|\mathbf{r}_\mathrm{P} - \mathbf{r}_\mathrm{Q}|$ is the optical path length between P and Q, n is the index of refraction, and we neglect the $1/r$ dependence of the amplitude. The wave propagates in the

#23554 - $15.00 US Received September 12, 2000; Revised October 17, 2000

general z-direction. The factor $A(\mathrm{P})$ represents the field amplitude and phase at the object point. For an extended object, the field at Q is proportional to the wavelet field integrated over all the object points:

$$E_k(Q) \sim \int_{\mathrm{p}} d^3\mathbf{r}_{\mathrm{p}} A(\mathrm{P}) \exp\left(ikr_{\mathrm{p}}\right). \tag{1}$$

The factor $\exp(ikr_P)$ represents the propagation and diffraction of the object wave. Now suppose that a number of copies of the electric field are generated by variation of the wave numbers k (or wavelengths λ), with all other conditions of object and illumination remaining the same. Then the resultant field at Q is

$$E(Q) \sim \sum_k \int_{\mathrm{p}} d^3\mathbf{r}_{\mathrm{p}} A(\mathrm{P}) \exp\left(ikr_{\mathrm{p}}\right) \sim \int_{\mathrm{p}} d^3\mathbf{r}_{\mathrm{p}} A(\mathrm{P}) \delta\left(\mathbf{r}_{\mathrm{p}} - \mathbf{r}_{\mathrm{Q}}\right) \sim A(\mathrm{Q}). \tag{2}$$

That is, for a large enough number of wave numbers k, the resultant field is proportional to the field at the object and is nonzero only at object points. In practice, if one uses a finite number N of wavelengths at regular intervals of $\Delta\lambda$, then the object image $A(\mathrm{P})$ repeats itself at axial distances $\Lambda = \lambda^2/\Delta\lambda$, with axial resolution $\delta = \Lambda/N$. By use of appropriate values of $\Delta\lambda$ and N, the axial period Λ can be matched to the axial extent of the object, and δ to the desired level of axial resolution. Note that for a given level of axial resolution δ, the required range of wavelengths $N\Delta\lambda$ is the same as the spectral width of low-coherence or short-pulse lasers in optical coherence tomography. A related technique of scanned wavelength and Fourier transform has been applied to imaging of first-arrival light in a scattering medium[10].

3. Experimental methods

The experiments are performed using a standard holographic apparatus shown schematically in Fig. 1. Approximately 50 mW of ring dye (RDL) laser's output is expanded to about 10 mm diameter and spatially filtered (BX). The object beam is apertured to about 5 mm diameter and illuminates the sample object. The scattered light from the object (OBJ) is

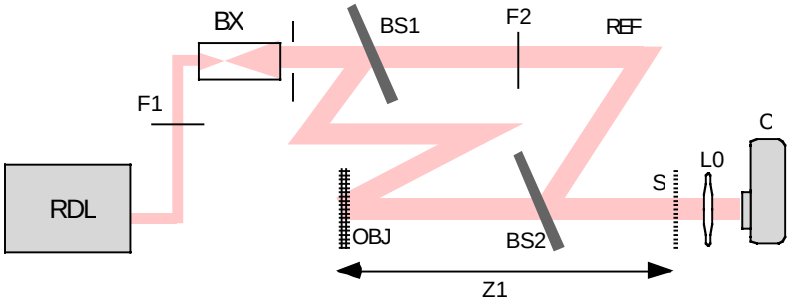

Fig. 1. The apparatus for digital interference holography. RDL: ring dye laser; F1 and F2: neutral density filters; BX: beam expander and spatial filter; BS1 and BS2: beam splitters; REF: reference beam; OBJ: object beam; S: camera's focal plane; LO: magnifying lens; C: digital camera; Z1: object to hologram distance

combined with the reference (REF) beam. The magnifying lens (LO) images the optical field at S onto infinity. The digital camera (C, Kodak DC290) is focussed at infinity, so that it records a magnified image of the optical intensity at the plane S. The object to hologram distance Z_1 is 195 mm. It is quite important to aperture the object beam so that it only illuminates the area of the object that is to be imaged, otherwise spurious scattering can seriously degrade reconstructed image's contrast and resolution[11]. A specimen of damselfly is used as the object, Fig. 2a). At a given laser wavelength, three images are

#23554 - $15.00 US Received September 12, 2000; Revised October 17, 2000

recorded: the hologram of object and reference interference (HH* = $|O+R|^2$), Fig. 3a); the object only (OO*), Fig. 3b); and the reference only (RR*), Fig. 3c). The laser wavelength is then stepped starting from $\lambda_0 = 601.7$ nm at $\Delta\lambda = 0.154$ nm intervals for $N = 20$ steps, so that the expected axial range is $\Lambda = 2.35$ mm and axial resolution $\delta = 0.12$ mm.

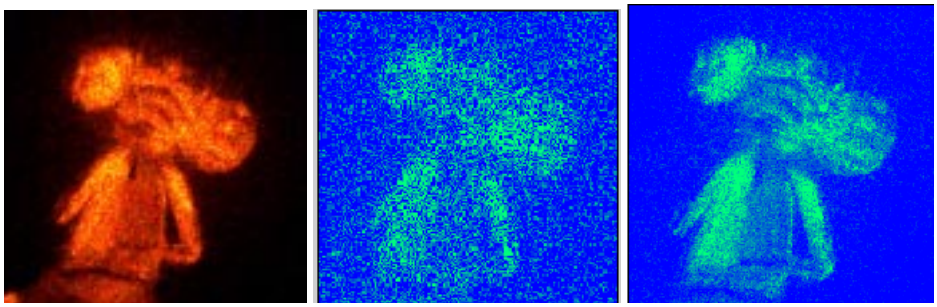

a) b) c)

Fig. 2. a) Direct camera image of the insect under laser illumination. The eyes, the mouthpiece, and the front two or three legs are visible. b) Numerically reconstructed image from one hologram. c) Image accumulated from the 20 holograms, as described in the text.

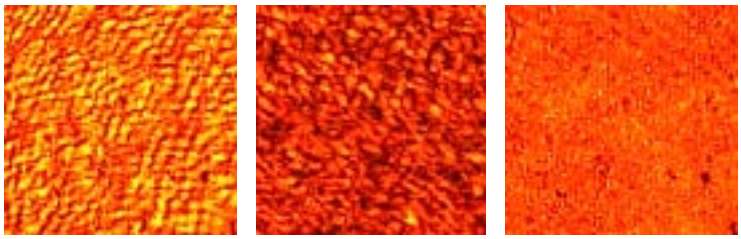

a) b) c)

Fig. 3. Digitally recorded optical fields, showing 1 x 1 mm details out of 4.8 x 4.8 mm frames: a) hologram, HH*, b) object, OO*, and c) reference, RR*.

The digitally recorded images are transferred to a computer, where a set of MatLab® scripts are used for numerical reconstruction. A 4.8 x 4.8 mm area of the image is interpolated to 512 x 512 pixel matrix. (The image magnification and interpolation are not an essential part of the experimental method but are necessitated because of the use of a digital camera instead of a bare CCD array.) The object and reference frames are then numerically subtracted from the hologram frame, HH* – OO* – RR*, before applying Fresnel diffraction. This is done to eliminate zero order diffraction and one obtains clean holographic images even at 0º offset between object and reference beams. This presumably leaves twin conjugate images RO* and R*O, but one of these is completely out of focus and apparently does not cause problem in our experiments. The holographic image field is calculated using Fresnel diffraction formula:

$$E(x,y;z) = \exp\left[\frac{ik}{2z}\left(x^2+y^2\right)\right] F\left\{E_0(x_0,y_0)S(x_0,y_0;z)\right\}\left[\kappa_x,\kappa_y\right] \qquad (3)$$

where

$$S(x,y;z) = -\frac{ik}{z}\exp\left[ikz+\frac{ik}{2z}\left(x^2+y^2\right)\right], \qquad (4)$$

$\kappa_x = kx/z,\ \kappa_y = ky/z,$ and $F\{f\}[\kappa]$ stands for Fourier transform of f with respect to the variable κ. The numerical reconstruction and digital interference proceeds as follows. Starting from a 512x512 pixel 4.8x4.8 mm digital hologram (with zero-order subtraction), the Fresnel

#23554 - $15.00 US Received September 12, 2000; Revised October 17, 2000

diffraction patterns are calculated at N+1 = 21 z-values, $z = Z_1 + m\delta$, where Z_1 = 195 mm is the original object distance and m = –10, –9, ... , 9, 10. This results in a 3D array of 512 x 512 x 21 pixel and 4.8 x 4.8 x 2.35 mm volume, that represents holographic optical field variation in this volume. The process is repeated for 20 sets of triple digitally recorded images at 20 different wavelengths. At this point, the field patterns in the individual 3D arrays show little variation along a few millimeters of z-direction. Now the twenty 3D arrays are numerically superposed together, by adding the arrays elementwise, resulting in the accumulated field array of the same size. This new array then has field distribution that represents the three-dimensional object structure, as described above. In practice, due to the laser's frequency fluctuation and imprecision of wavelength intervals, there is always a random phase variation among the twenty calculated field arrays. This is readily corrected by introducing a global phase factor to each of the 3D arrays before carrying out the summation. Additional details on the optical and numerical experiments and their variations will be reported later.

4. Results and analysis

Figure 2b) is an example of 2D holographic image reconstructed from a single hologram at Z_1 = 195 mm. Imaging of diffuse scattering objects, such as this biological specimen, using coherent illumination gives rise to the speckle noise, causing degradation of contrast and resolution. This can be reduced to certain extent by being extra cautious with illumination aperture and overall stability of the optical system. Now we demonstrate the effect of digital interference, in Fig. 4. The animation frames show a 2.35 x 4.8 mm z-y cross section at x = –1.3 mm, as the holographic field arrays are added on top of each other from one two twenty. When N = 1, the z-variation is only due to little noticeable diffraction of the field, but at N = 2 the field exhibits cosine variation in the z-direction, with different phase origin depending on the object surface distance. As more and more arrays are added, the cosine pattern becomes similar to delta-function spikes in the z-direction. When all 20 field arrays are accumulated, only one z-value has large intensity above noise, for each object surface pixel.

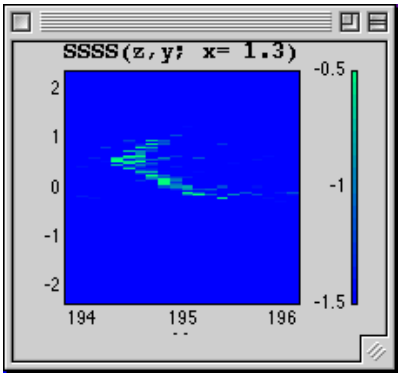

Fig. 4. (QuickTime, 504k) The animation shows a z-y cross section of the 3D reconstructed field at x = –1.3 mm, as the twenty 3D arrays are added in digital interference holography.

Figure 5 shows various cross sectional, tomographic, views of the accumulated field array. Figure 5a) shows x-y cross sections as the axial distance z is varied from the front tip of the mouth piece to the back of the eyes, over a distance of 2.35 mm. Figure 5b) shows z-y cross sections as the x-value is varied from 1.84 to 0.52 mm, or from the edge of the insect's left eye to the middle of the face. The contrast of these images has been numerically enhanced by applying logarithm and thresholds to the calculated field arrays. The tomographic imaging by wavelength-scanning digital interference is quite clearly demonstrated. The accumulation of N holographic field arrays has an additional significant benefit of averaging out the coherent speckle noise. Figure 2c) is obtained by starting from the accumulated array and summing over the z-direction, yielding a 2D image of the object. The resulting image quality

#23554 - $15.00 US Received September 12, 2000; Revised October 17, 2000

approaches that of the photographic image and the speckle noise is almost completely removed. Furthermore, each object surface element is imaged in focus regardless of the depth of focus of the optical system, which will be of significant benefit when the technique is applied to microscopic imaging with large numerical aperture. Finally, we present in Fig. 6 an animated 3D reconstruction of the object's illuminated surface, by plotting the brightest voxels (volume elements) in 3D perspective. As the azimuthal angle rotates, one can recognize the two eyes and the mouth piece, as the most prominent features. Two or three front legs are also visible, although there seem to be some ghost images of these.

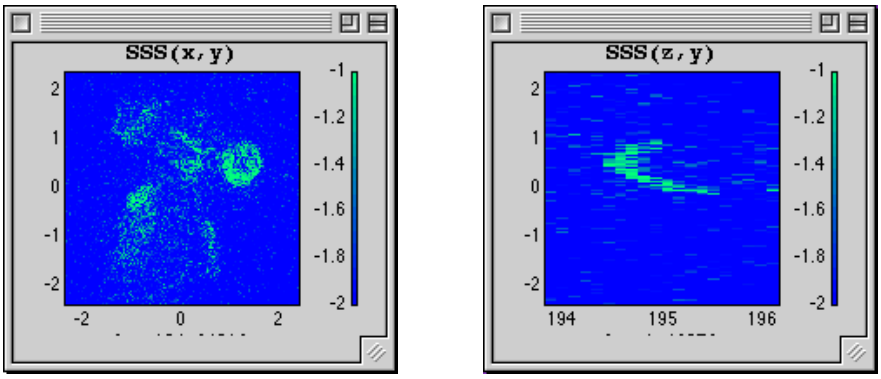

Fig. 5. a) (QuickTime, 504k) *x*-*y* cross sections of the accumulated array at various axial distances *z*. b) (QuickTime, 504k) *z*-*y* cross sections of the accumulated array at various *x*-values starting from left end of the head, $x = 1.84$ mm, to near the middle of the head, $x = 0.52$ mm.

Fig. 6. (QuickTime, 756k) An animated 3D reconstruction of the insect's illuminated surface. (Here the insect is facing upward, the vertical being the z-axis.)

5. Conclusions

The experiment presented here demonstrates three-dimensional imaging of a mm-sized biological specimen using the wavelength-scanning digital interference holography. The technique is capable of generating cross-sectional images of the object with clear focus and good suppression of coherent speckle noise, using fairly simple optical system and straightforward numerical methods. The achieved resolution is ~100 μm in the axial direction and ~20 μm in the lateral direction, which are limited only by the present optical system and computer capacity. When the set up is scaled down to semi-transparent microscopic objects, full tomographic imaging of internal structures will be possible.

#23554 - $15.00 US Received September 12, 2000; Revised October 17, 2000